

## Experimental and Theoretical Study of Nitric Oxide Formation in Internal Combustion Engines

GEORGE A. LAVOIE, JOHN B. HEYWOOD, AND JAMES C. KECK

*Massachusetts Institute of Technology, Cambridge, Massachusetts*

**Abstract**—The nonequilibrium formation of nitric oxide within the internal combustion engine cylinder is examined. A thermodynamic model which predicts the properties of the burnt and unburnt gases during the combustion process is developed. A set of reactions which govern the formation of nitric oxide is proposed, and rate equations for nitric oxide concentrations as a function of time in the post-flame gases are derived. The results of time-resolved measurements carried out on a CFR engine are described, where emitted light intensities at wavelengths selected to record radiation from the  $\text{CO} + \text{O}$  and  $\text{NO} + \text{O}$  continua were used to determine the nitric oxide concentration. The comparison between theoretical and experimental results for fuel-lean mixtures confirms that the important features of the model presented are correct.

### I. INTRODUCTION

It is now accepted that nitric oxide in the exhaust gases of combustion devices is one of the pollutants which react in the atmosphere to form photochemical smog. The automobile is the largest single source of nitric oxide. It contributes about 50 per cent overall of the total emitted, though in the Los Angeles basin, where the smog problem is most severe, its contribution is significantly higher. The processes which govern the production of nitric oxide inside the engine cylinder are not well understood, however. Since legislation which will limit the amount of nitric oxide which automobile engines can exhaust into the atmosphere is anticipated in the near future, a more basic understanding of the production mechanism is essential.

Most of the previous work on nitric oxide production has involved correlations of nitric oxide concentrations measured in the exhaust gases with the engine operating parameters such as fuel/air ratio, spark advance, engine speed, exhaust manifold pressure (e.g., Huls and Nickol (1967), Hazen and Holiday (1962), Alperstein and Bradow (1966), Wimmer and McReynolds (1961)). From such studies a qualitative understanding of the process has been built up. For example, modifications in engine operating conditions which increase the peak cycle temperature, or the oxygen concentration in the burnt gases increase the nitric oxide concentration in the exhaust. The measured nitric oxide levels are found to be nearer the equilibrium concentration corresponding to the peak cycle temperature and pressure, than to the equilibrium concentration at exhaust conditions.

Two previous papers have proposed possible

kinetic schemes to account for this nonequilibrium concentration. Newhall and Starkman (1967) using a kinetic model based on the Zeldovich mechanism, Zeldovich (1946), with O and N assumed in equilibrium with  $\text{O}_2$  and  $\text{N}_2$ , respectively, predicted immediate freezing of the assumed equilibrium composition at the peak temperature and pressure for homogeneous burnt gases. Their time-resolved spectroscopic measurements at  $5.3 \mu$  gave nitric oxide concentrations considerably in excess of equilibrium concentrations at the peak pressure and temperature; their measurements also showed no decomposition during the expansion stroke. Later Newhall (1968) with calculations using a more detailed kinetic model again predicted the freezing of nitric oxide at the assumed peak equilibrium concentration. Eyzat and Guibet (1968) considered the formation process. They assumed nitric oxide was formed by the reaction  $\text{N}_2 + \text{O}_2 \rightarrow 2\text{NO}$  and carried out kinetic calculations using a perfect gas model for the thermodynamic properties of the unburnt and burnt gases, with the burnt gases taken to be homogeneous. They concluded that in fuel-lean mixtures the formation process was too slow for nitric oxide to reach equilibrium at the peak pressure and temperature. However, the reaction used to follow the formation of nitric oxide does not proceed directly and is not the rate determining reaction.

The following questions concerning nitric oxide production in the engine cylinder still remain unanswered. Firstly, what is the state of the combustion products? No account has yet been taken of nonuniformities in the post-flame gases. It is known, Rassweiler and Withrow (1935), that a

substantial temperature gradient ( $\Delta T \sim 200$  °K) exists due to the different time histories of gas elements which burn early or late in the combustion process. Such temperature differences would be expected to result in substantial nonuniformity in nitric oxide concentration. Secondly, what reactions must be included in the nitric oxide kinetic scheme to follow both formation and decomposition? A related question is whether nitric oxide formation within the flame front is important compared with the rate-limited processes occurring in the post-flame gases? The third question concerns experimental verification of the theoretical model. Since nitric oxide formation is a nonequilibrium process, the details can only be confirmed with time-resolved measurements of the nitric oxide concentration within the engine cylinder.

In this study, which is directed at these three problem areas, our approach is based on the following assumption. In general, the rates of the energy-producing reactions in a flame are sufficiently fast so that the burned gases are close to thermodynamic equilibrium. This permits us, in our theoretical model, to separate the problem of nitric oxide formation into two parts: The first involves the determination of the temperature, density, and concentration of major species in the burned gas assuming that the carbon-oxygen-hydrogen system is in equilibrium; the second involves integration of the reaction rate equations for nitric oxide in the previously determined environment.

## II. THERMODYNAMICS OF INTERNAL COMBUSTION

At the temperature and densities in an internal combustion engine, it is a reasonable first approximation to assume that the volume of the reaction zone is negligible and that the gas within a cylinder consists of a burned fraction at thermodynamic equilibrium plus an unburned fraction frozen at its original composition. If we also assume that the pressure is uniform throughout the cylinder, then the conditions in the burned and unburned gases are determined by the equation of state for the burned gas

$$pv_b = R_b T_b, \quad (1)$$

the equation of state for the unburned gas,

$$pv_u = R_u T_u, \quad (2)$$

conservation of mass,

$$V/M = \int_0^x v_b dx' + \int_x^1 v_u dx', \quad (3)$$

and conservation of energy,

$$(E - W - Q)/M = \int_0^x e_b dx' + \int_x^1 e_u dx', \quad (4)$$

where  $p$  is the pressure,  $v$  is the specific volume,  $R$  is the gas constant,  $T$  is the temperature,  $V$  is the cylinder volume,  $M$  is the mass of gas in the cylinder,  $x$  is the mass fraction burned,  $E$  is the total energy,  $W$  is the work done on the piston,  $Q$  is the heat loss,  $e$  is the specific internal energy, and the subscripts  $b$  and  $u$  refer to burned and unburned gas, respectively.

In general equations (3) and (4) form a set of coupled integral equations which cannot be solved analytically. However, over the temperature ranges of interest, it is a reasonable approximation to assume constant specific heats for both burned and unburned gases. Under these conditions

$$e_b = c_{vb} T_b + h_{fb}, \quad (5)$$

and

$$e_u = c_{vu} T_u + h_{fu}, \quad (6)$$

where  $c_{vb}$ ,  $c_{vu}$ ,  $h_{fb}$  and  $h_{fu}$  are constants obtained by fitting straight lines to the specific energy versus temperature curves.

Substituting equations (1), (2), (5) and (6) into (3) and (4), we obtain

$$pV/M = xR_b \bar{T}_b + (1-x)R_u \bar{T}_u \quad (7)$$

and

$$(E - W - Q)/M = x(c_{vb} \bar{T}_b + h_{fb}) + (1-x) \times (c_{vu} \bar{T}_u + h_{fu}) \quad (8)$$

where

$$\bar{T}_b = \left( \int_0^x T_b dx' \right) / x \quad (9)$$

and

$$\bar{T}_u = \left( \int_x^1 T_u dx' \right) / (1-x) \quad (10)$$

are the mean temperatures of the burned and unburned gases. Equations (7) and (8) may now be solved to obtain

$$Mx = \frac{pV - p_0 V_0 + (\gamma_b - 1)(W + Q) + (\gamma_b - \gamma_u) M c_{vu} (\bar{T}_u - T_0)}{(\gamma_b - 1)(h_{fu} - h_{fb}) + (\gamma_b - \gamma_u) c_{vu} \bar{T}_u} \quad (11)$$

and

$$R_b \bar{T}_b = R_u \bar{T}_u + (pV - MR_u \bar{T}_u)/Mx, \quad (12)$$

where  $\gamma = c_p/c_v$  is the specific heat ratio, and the subscript 0 refers to any convenient reference state

prior to ignition for which  $x = 0$ . Note that by definition

$$\rho_0 V_0 = MR_u T_0 \quad (13)$$

and

$$W = \int_{V_0}^V p dV'. \quad (14)$$

If we now assume the unburned gas is initially uniform and undergoes isentropic compression then

$$\bar{T}_u/T_0 = (p/p_0)^{(\gamma_u-1)/\gamma_u}. \quad (15)$$

This equation together with equations (11) and (12) enables one to determine both  $x$  and  $\bar{T}_b$  from the thermodynamic properties of the burned and unburned gases and measured values of  $p$ ,  $V$ ,  $M$  and  $Q$ . We will take  $Q$  to be zero in the subsequent analysis.

To proceed further, we must make some assumptions about conditions in the burned gas, and we shall consider two limiting cases. In the first case, we assume the temperature of the burned gas is uniform so that  $T_b = \bar{T}_b$ . The state of the burned gas is then given by equations (1), (11), (12) and (15). This case corresponds to infinite heat conductivity in the burned gas. We will also assume the burned gas composition is uniform, which corresponds to a "fully mixed" model and represents one limiting condition. In the second case, we assume that no mixing of the burned gases occurs, and each gas element is isentropically compressed after combustion so that

$$T_b(x', x)/T_b(x') = [p(x)/p(x')]^{\gamma_b-1/\gamma_b}, \quad (16)$$

where  $T_b(x', x)$  is the temperature of the element which burned at the pressure  $p(x')$ , when the pressure is  $p(x)$ ; and

$$T_b(x') = [h_{fu} - h_{fb} + c_{pu}\bar{T}_u(x')]/c_{pb} \quad (17)$$

is the temperature resulting from the isenthalpic combustion of the gas at the pressure  $p(x')$ . Equations (16) and (17) together with (1), (11) and (15) then give the state of the burned gas. This case corresponds to zero heat conductivity in the burned gas, and no mixing. This "unmixed" case represents the opposite limit to the "fully mixed" case, and in view of well-known measurements of the temperature gradient existing in the burned gases, is probably closer to reality.

The above equations have been programmed for solution on a digital computer. In addition, computer programs have been developed to calculate the required thermodynamic properties for

both equilibrium and frozen mixtures of fuel, air, and combustion products containing up to fifty species.

Some examples of results for the CFR engine used in the experiments discussed in Section V are shown in Figures 1 and 2. Figure 1 shows a measured pressure curve and the corresponding mass fraction burned as functions of crank angle  $\theta$ . Engine conditions were equivalence ratio,  $\phi = 0.9$ , engine speed  $N = 1200$  rpm and residual fraction  $\varepsilon = 0.05$ . Measurements of oxygen concentration in the exhaust confirm that the charge was not completely burned. As described in Section V(i), the special cylinder head was designed for ease of optical measurements, and as a result high combustion efficiency has been sacrificed. The decay in  $x$  after the maximum results from the constant  $\gamma_b$  assumption, with the value of  $\gamma_b$  chosen to match equilibrium data over a range of temperatures.

Figure 2 illustrates the difference between the "mixed" and "unmixed" models. It shows, as a function of  $x$  the mass fraction burned: (i) the

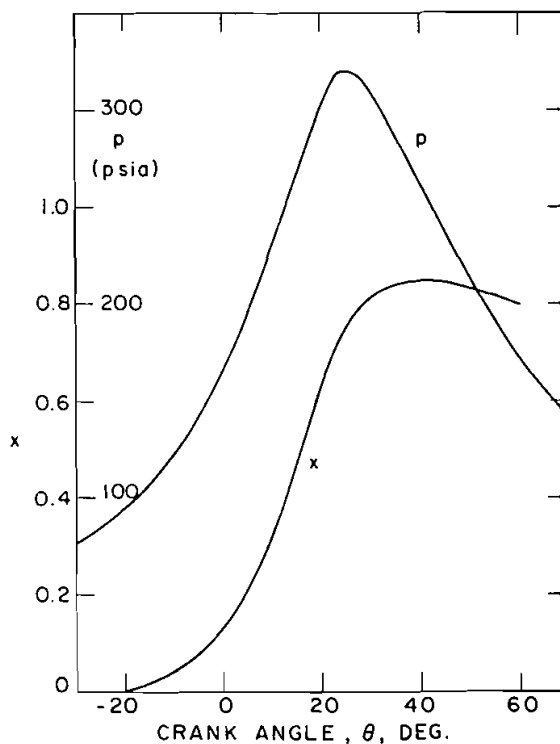


FIG. 1. Measured pressure,  $p$ , and calculated mass fraction burned,  $x$  as functions of crank angle,  $\theta$ . Conditions are equivalence ratio 0.9, engine speed 1200 rpm, residual fraction 0.05.

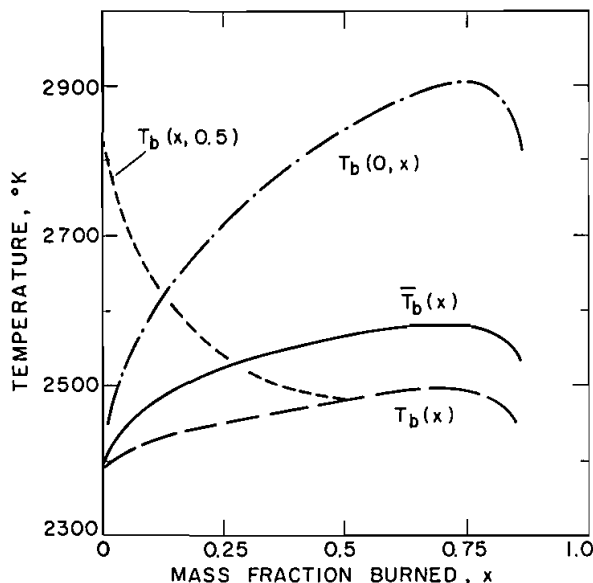
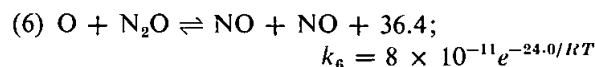
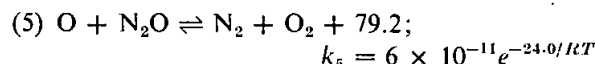
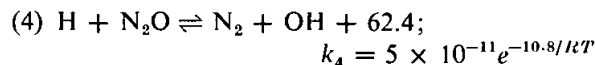
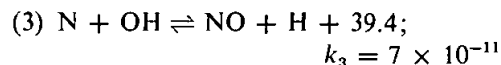
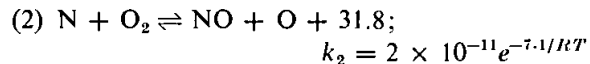
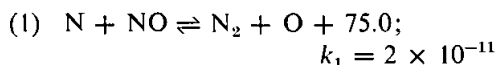


FIG. 2. Calculated temperature distributions in the burned gas for mixed and unmixed models: (i) The mean temperature of the burned gas,  $\bar{T}_b(x)$ ; (ii) the temperature of the element burned at  $x$ ,  $T_b(x)$ ; (iii) the temperature of the first element burned,  $T_b(0, x)$ ; (iv) the temperature distribution for the unmixed case when half the charge is burned,  $T_b(x, 0.5)$ .

mean temperature of the burned gas,  $\bar{T}_b(x)$ ; (ii) the temperature of the element burned at  $x$ ,  $T_b(x)$ ; (iii) the temperature of the first element burned  $T_b(0, x)$ ; and (iv) the temperature distribution for the unmixed case at a time when half the gas is burned,  $T_b(x, 0.5)$ . Note that the unmixed model predicts that the temperature of the first element burned is substantially higher than the mean temperature and that when the charge is fully burnt, a temperature difference of about 400 °K exists across the post-flame gases.

### III. KINETICS OF NITRIC OXIDE FORMATION

The process of nitric oxide formation in various gases has been extensively studied in shock tubes, flow systems, and flames, and rate constants for the important reactions have been determined. This work indicates that, under conditions prevailing in internal combustion engines, the process will be governed primarily by the following reactions:



where the exothermicities of the reactions are given in kcal, the exothermic rate constants  $k_i$ , are given in  $\text{cm}^3 \text{sec}^{-1}$ , and the activation energies are given in kcal. The rate constants are taken from Schofield (1967) for reactions 1, 2, 4, 5 and 6, and from Campbell (1968) for reaction 3. Note that we have not included the reaction  $2\text{NO} \rightleftharpoons \text{N}_2 + \text{O}_2$  which is very slow and does not proceed directly.

In the present investigation, we are considering only the processes occurring in the burned gas behind the reaction zone. The rates of the energy-producing reactions in a flame are sufficiently fast so that the burned gases are close to thermodynamic equilibrium.\* We may therefore assume equilibrium concentrations for O,  $\text{O}_2$ , H, OH and  $\text{N}_2$ . The rate equations for the remaining species NO, N, and  $\text{N}_2\text{O}$  can then be written in the form:

$$\frac{1}{V} \frac{d[\text{NO}]V}{dt} = -\alpha(\beta R_1 + R_2 + R_3 + 2\alpha R_6) + R_1 + \beta(R_2 + R_3) + 2\gamma R_6 \quad (18)$$

$$\frac{1}{V} \frac{d[\text{N}]V}{dt} = -\beta(\alpha R_1 + R_2 + R_3) + R_1 + \alpha(R_2 + R_3) \quad (19)$$

$$\frac{1}{V} \frac{d[\text{N}_2\text{O}]V}{dt} = -\gamma(R_4 + R_5 + R_6) + R_4 + R_5 + \alpha^2 R_6. \quad (20)$$

$R_i$  is the "one-way" equilibrium rate of the  $i$ th reaction (e.g.,  $R_1 = k_1[\text{N}]_e[\text{NO}]_e$  with subscript  $e$  denoting equilibrium concentration); and  $\alpha = [\text{NO}]/[\text{NO}]_e$ ,  $\beta = [\text{N}]/[\text{N}]_e$ , and  $\gamma = [\text{N}_2\text{O}]/[\text{N}_2\text{O}]_e$ , i.e., the concentration of NO, N and  $\text{N}_2\text{O}$  divided by their equilibrium concentration.  $V$  is the volume

\* This assumption may not be satisfactory towards the end of the expansion stroke. However, we shall show that nitric oxide levels freeze early in the expansion stroke so the error will not be significant.

of the burned gas: For the unmixed case  $V$  is the volume of a small gas element of fixed mass; for the fully mixed case  $V$  is the total volume of burned gas in the cylinder, and its mass increases with time.

Rough estimates of the magnitude of the terms in equations (18), (19) and (20) indicate that the relaxation times for equations (19) and (20) are several orders of magnitude shorter than that of equation (18). It is therefore an excellent approximation to assume steady-state concentrations for N and  $N_2O$  and set the right-hand sides of equations (19) and (20) equal to zero. We can then eliminate  $\beta$  and  $\gamma$  from equation (18), and the equation for nitric oxide formation becomes

$$\frac{1}{V} \frac{d[\text{NO}]V}{dt} = 2(1 - \alpha^2) \left( \frac{R_1}{1 + \alpha K_1} + \frac{R_6}{1 + K_2} \right) \quad (21)$$

where  $K_1 = R_1/(R_2 + R_3)$  and  $K_2 = R_6/(R_4 + R_5)$ . Note that we have not assumed N is in equilibrium with  $N_2$  through the dissociation reaction  $N_2 + M \rightleftharpoons N + N + M$ . This reaction is too slow to bring N into equilibrium at the pressures and temperatures of interest.

The first term in the large brackets on the right side of equation (21) is the result of reactions (1)–(3). It corresponds to the Zeldovich mechanism extended by adding the reaction between N and OH. The second term is the result of reactions (4)–(6) which involve  $N_2O$  as an intermediary. It is this term which under some conditions is kinetically equivalent to the  $2\text{NO} \rightleftharpoons N_2 + O_2$  reaction.

Values of  $K_1$  and  $K_2$  are given in Table I for a range of temperatures and equivalence ratios. In general  $K_1$  and  $K_2$  are of order unity or less, and thus for small  $\alpha$  the relative importance of the two mechanisms just described is determined by the

TABLE I

(a) Values of $K_1$			
	$\phi = 0.8$	1.0	1.2
$T = 3000^\circ\text{K}$	0.3	0.3	0.2
2500	0.4	0.3	0.1
2000	0.4	0.4	0.06
1500	0.1	0.8	0.02
(b) Values of $K_2$			
	$\phi = 0.8$	1.0	1.2
$T = 3000^\circ\text{K}$	0.3	0.2	$5 \times 10^{-2}$
2500	0.4	$8 \times 10^{-2}$	$5 \times 10^{-3}$
2000	0.5	$3 \times 10^{-2}$	$7 \times 10^{-5}$
1500	0.8	$5 \times 10^{-3}$	$4 \times 10^{-8}$

TABLE II

Values of $R_6/R_1$	$\phi = 0.8$	1.0	1.2
$T = 3000^\circ\text{K}$	$4 \times 10^{-2}$	$1 \times 10^{-2}$	$1 \times 10^{-2}$
2500	$9 \times 10^{-2}$	$3 \times 10^{-2}$	$4 \times 10^{-3}$
1000	$5 \times 10^{-1}$	$5 \times 10^{-2}$	$9 \times 10^{-4}$
1500	6	$1 \times 10^{-1}$	$5 \times 10^{-5}$

ratio of  $R_6$  to  $R_1$ . Values of  $R_6/R_1$  are given in Table II. It can be seen that, except for lean mixtures at low temperatures, most of the nitric oxide formation will occur via the extended Zeldovich mechanism. During the removal process, however, when  $\alpha$  becomes very large, the  $N_2O$  mechanism may become dominant. On the time scale of interest, this has relatively little effect since both mechanisms are slow and effectively frozen. The  $N_2O$  mechanism does become important in nitric oxide formation in furnaces where lower temperatures and excess air are the norm. Reaction (3) affects the value of  $K_1$ ; in rich mixtures the value of  $K_1$  can be significantly reduced.

#### IV. CALCULATION OF NITRIC OXIDE CONCENTRATIONS IN THE BURNED GAS

Equations (18)–(20) and equation (21) have been programmed for integration on a digital computer. The required equilibrium reaction rates, equilibrium compositions, and thermodynamic properties are obtained from a thermodynamic equilibrium computer program. The results obtained for internal combustion engine conditions confirm that the steady-state approximation is valid, and hence only a solution to equation (21) is required. The integration of equation (21) is linked with the thermodynamic model of the combustion process in the following way. We will consider only the unmixed case.

The path followed by each element burnt is shown in Figure 3. Consider the element that burns at  $p_i$ . For  $p < p_i$  it is compressed along the isentrope  $S_u$  to state  $(p_i, h_i)$ . After isenthalpic combustion its entropy is  $S_{bi}$ , and since no mixing occurs, the element is further compressed along the isentrope  $S_{bi}$ . Element  $j$  which burns at a later time is compressed along the isentrope  $S_{bj}$  after combustion. Due to the difference in specific heats of burnt and unburnt gases, it has a lower temperature than element  $i$ . Thus given  $p_i$  and  $h_i$ , and  $p$  as a function of time,  $S_{bi}$  is computed, and the state-time history of the element obtained. Equation (21) can now be integrated along  $S_{bi}$ .

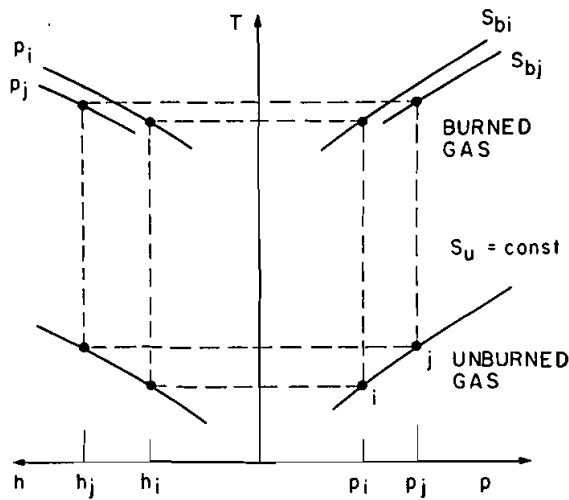


FIG. 3. Illustration of calculation procedure for nitric oxide concentration in unmixed case on pressure-temperature-enthalpy plot.

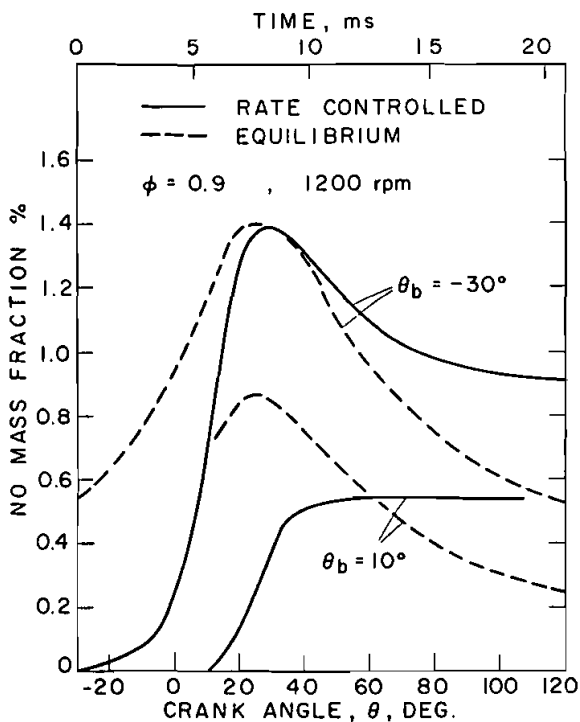


FIG. 4. Nitric oxide mass fractions as a function of time in the burnt gas for two elements which burn at different times.  $\theta_b = -30^\circ$  is the first part of the charge to burn; at  $\theta_b = 10^\circ$ , one third of the charge is burnt. Equivalence ratio is 0.9, engine speed is 1200 rpm, residual fraction is 0.05.

Typical results for nitric oxide mass fractions in the burnt gas for two elements which burn at different times are shown in Figure 4. The equivalence ratio is 0.9, the engine speed 1200 rpm, the residual fraction is 0.05.  $\theta_b = -30^\circ$  is the first part of the charge to burn; at  $\theta_b = 10^\circ$ , about one-third of the charge is burnt. Equilibrium nitric oxide concentrations corresponding to the local temperature and pressure are also shown. Note that freezing occurs in the rate-controlled solutions early in the expansion stroke. Whether the rate-controlled solution reaches nitric oxide concentrations equal to the equilibrium value at the peak temperature (e.g., the  $\theta_b = -30^\circ$  solution) will depend on the temperatures attained and the engine speed.

The average exhaust nitric oxide concentration is obtained from the integral

$$\overline{\{\text{NO}\}_f} = \int_0^1 \{\text{NO}\}_f dx, \quad (22)$$

where  $\{\text{NO}\}_f$  denotes the frozen nitric oxide mass fraction of the element which burned at  $x$ . Figure 5 shows  $\{\text{NO}\}_f$  as a function of  $x$  for  $\phi = 0.9$ . The exhaust concentration is predicted to be about 4000 ppm. Note that the first part burned has six times the frozen nitric oxide concentration of the last part burned.

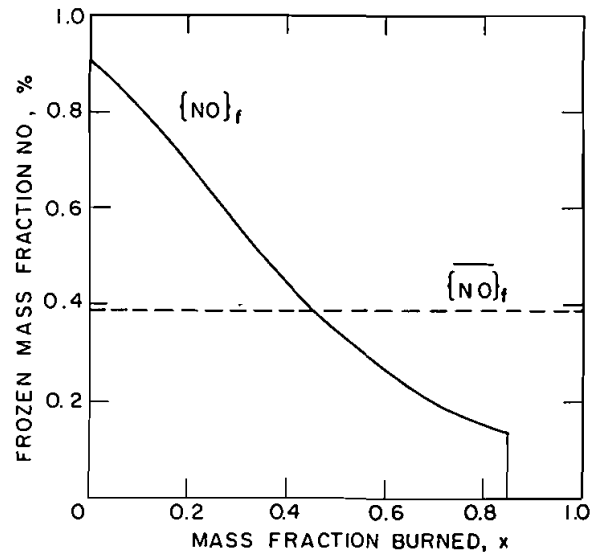


FIG. 5. Frozen nitric oxide mass fraction as a function of value of  $x$  at which element burned. Integrated value gives exhaust concentration.

## V. TIME-RESOLVED MEASUREMENTS OF NITRIC OXIDE CONCENTRATION

### 1. Method and Experimental Equipment

To investigate nitric oxide concentrations in an operating engine cylinder, we have employed time-resolved spectroscopic techniques. Briefly, the method involves the simultaneous measurement of light emission intensities at two wavelengths characteristic of the two recombination continua:  $\text{CO} + \text{O} \rightarrow \text{CO}_2 + h\nu$  and  $\text{NO} + \text{O} \rightarrow \text{NO}_2 + h\nu$ . The intensities are

$$I_{\text{CO}} = K_1(T)[\text{CO}][\text{O}] \quad \text{and} \quad I_{\text{NO}} = K_2(T)[\text{NO}][\text{O}]$$

where the  $K$ 's are known functions of temperature and wavelength; Hartunian *et al.* (1966), Myers and Bartle (1967), Fontijn *et al.* (1964). Using the assumption of equilibrium concentrations of species in the C—O—H system, described in Section II, the measurement of  $I_{\text{CO}}$  and the pressure  $p$  allows the determination of temperature  $T$ , carbon monoxide concentration  $[\text{CO}]$ , and oxygen atom concentration  $[\text{O}]$ . The measurement of  $I_{\text{NO}}$  then gives the nitric oxide concentration  $[\text{NO}]$ .

The experiments were conducted on a single cylinder, L-head, C.F.R. engine. A specially designed head allowed light emission measurements

to be made through a number of small quartz windows at different positions along the flame path. The engine head and combustion chamber are shown in Figure 6. Spark plug, window locations, and ports for the Li Strain Gauge pressure transducer are indicated. The engine compression ratio was 4.9, and the exhaust was pumped down to a pressure of 6 psia to improve the operating characteristics. Unleaded fuel was used.

The optical set up is shown in Figure 7. Radiation is emitted from a small volume of gas encompassed by a cone of light rays passing through a  $2 \times 2$  mm source area in the center of the combustion chamber. The light cone is split up by a four-part mirror  $M_2$ , into four quadrants each of which is brought to a separate focus by  $M_3$  and  $M_4$ . Three of the channels were monitored with photomultiplier-interference filter pairs; the channels at  $0.38 \mu$  and  $0.61 \mu$  had a band pass of  $100 \text{ \AA}$  while the channel at  $0.75 \mu$  had a band pass of  $300 \text{ \AA}$ . The fourth channel was monitored with a Jarrell-Ash model 82-000 monochromator and photomultiplier. The band pass could be varied from  $1.6 \text{ \AA}$  to  $22 \text{ \AA}$  depending on the slit width. The entire optical system was mounted in a solid frame which could be moved on rails to any window position. The entire optical system including the actual window used was calibrated before and after each

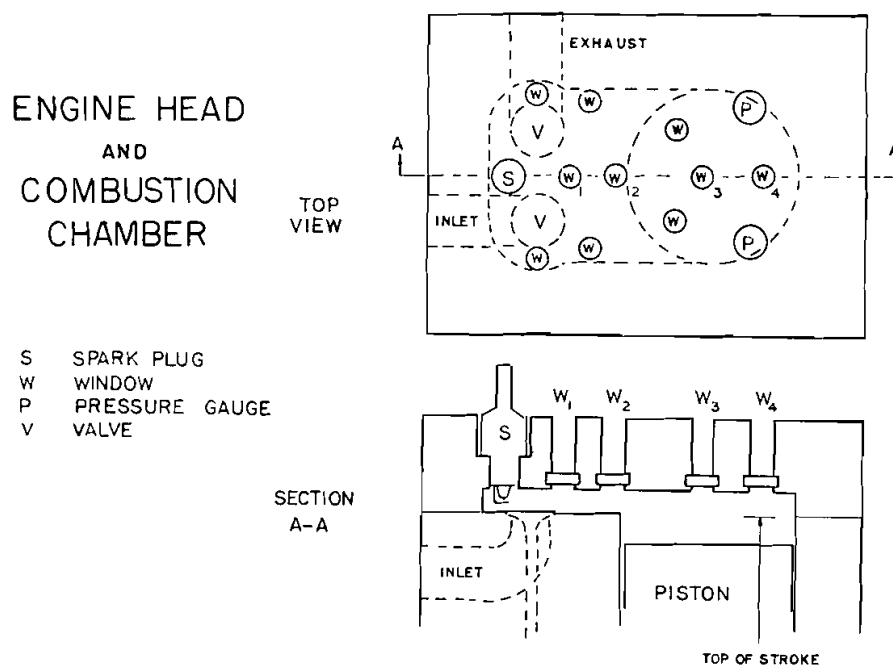


FIG. 6. Engine head and combustion chamber design for L-head, C.F.R. Engine.

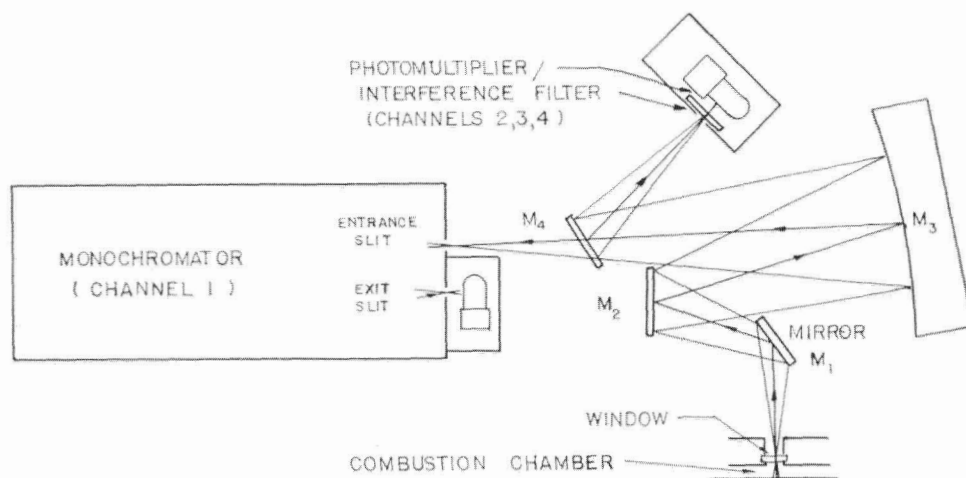
OPTICAL TRAIN  
SCHEMATIC

FIG. 7. Schematic of optical train.

run with a dummy window mount and a calibrated tungsten strip lamp.

In addition to photomultiplier output, the monochromator could be equipped with a camera to record the spectrum in intervals of 400 Å. The result of putting together a number of overlapping spectra is shown in Figure 8. The film was exposed continuously for some hundreds of cycles. The

upper spectrum was taken with a band pass of 1.6 Å on Polaroid 107 film; the lower has a band pass of 22 Å on Polaroid 413 infrared film. Except for some identifiable discrete line radiation, the spectrum consists of continuum radiation, suggesting the composition shown in Figure 9; the radiation is primarily due to the OH bands, and the CO<sub>2</sub> and NO<sub>2</sub> recombination continua. Quantitative

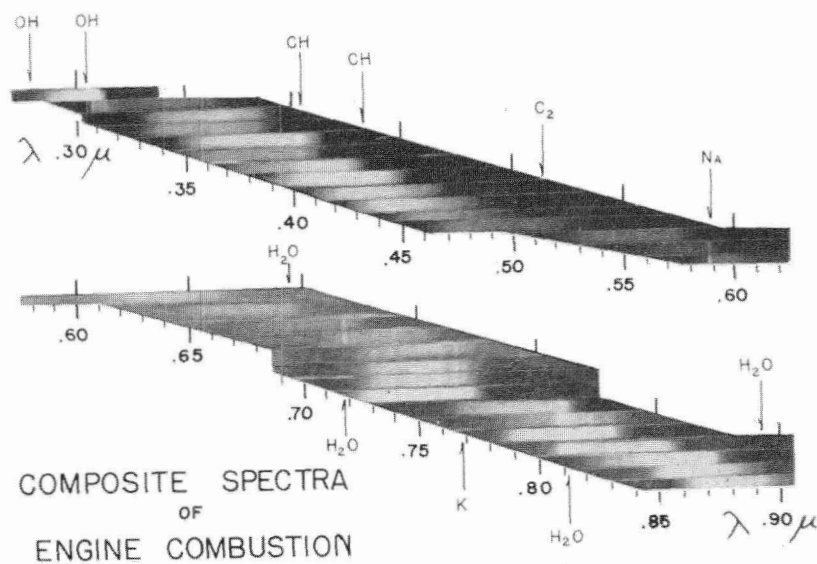


FIG. 8. Composite spectra of engine combustion showing prominent band heads and underlying continua obtained with continuous exposure for many engine cycles.

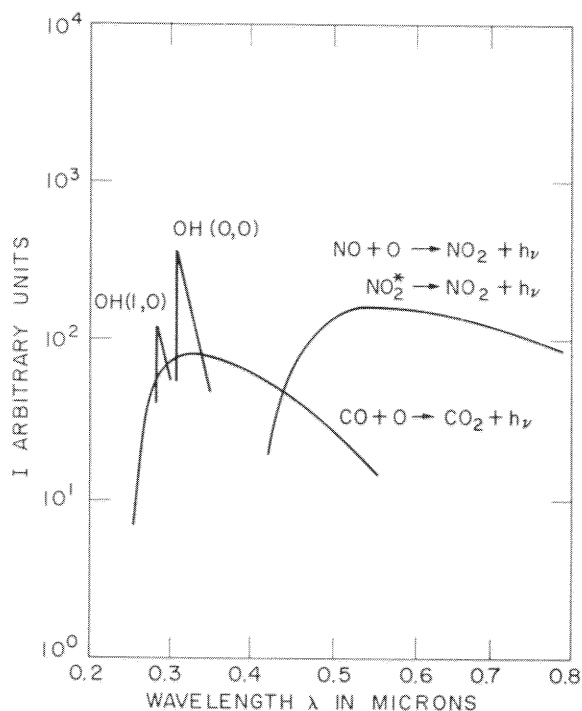


FIG. 9. Spectral shapes of major radiation components. Radiation intensity plotted against wavelength.

measurements with the four channel optical systems have verified this decomposition. Those measurements will be described next.

## 2. Verification of Nitric Oxide Measuring Technique

A typical oscilloscope record of a single cycle is shown in Figure 10; pressure, crank angle, and radiation intensity from three channels are displayed as a function of time. The spark time is indicated by the break in the pressure trace. No

TIME 2 MS/DIV  
 CRANK ANGLE  $\theta$   
 PRESSURE 50 psi/DIV  
 LIGHT INTENSITY  $I_{0.38 \mu}$   
 $I_{0.68 \mu}$   
 $I_{0.61 \mu}$

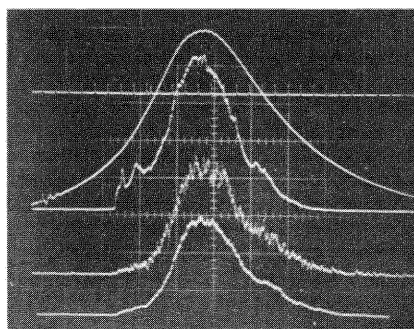


FIG. 10. Typical data record showing crank angle ( $5^\circ$  markers), pressure and radiation intensity at three wavelengths.

radiation is seen until the flame front reaches the window, then there is a sharp rise in signal followed by a short period ( $\sim 1.5$  ms) of fluctuations, seen here on the  $0.38 \mu$  channel, which is interpreted as defining a turbulent, nonequilibrium reaction zone.

It is also possible to display  $x - y$  behavior of light intensity at one wavelength versus intensity at another. Single cycle and superimposed multicycle records of this kind revealed that to  $\pm 15$  per cent the radiation in the wavelength range  $0.30 \mu$  to  $0.40 \mu$  was proportional to the radiation at  $0.38 \mu$ , while radiation between  $0.58 \mu$  and  $0.68 \mu$  was proportional to that at  $0.61 \mu$ . Then using simultaneous measurements of radiation at  $0.38 \mu$  and  $0.61 \mu$ , the spectral distribution can be plotted as in Figure 11 where the spectrum is shown at three consecutive times during the cycle, before, at, and after peak pressure for two fuel/air equivalence ratios,  $\phi = 1.2$  (20 per cent fuel rich) and  $\phi = 0.9$ .

Qualitatively, the spectrum shows the general shapes indicated previously: the OH(0,0) band and the continuum, whose behavior is consistent with a decomposition into CO and NO contributions. Since the two continua depend almost entirely on the products  $[\text{CO}][\text{O}]$  and  $[\text{NO}][\text{O}]$ , we see in the lean case that there is a transient growth of NO relative to CO which is consistent with the nonequilibrium behavior of nitric oxide predicted by the kinetic model. In the rich case the equilibrium CO concentrations are higher, and the O concentrations are lower, so that the CO—O continuum tends to dominate the emission although a small shift in the NO—O continuum is discernable.

In order to make the identification of the spectral components complete, two experiments were conducted. In the first, the radiation at  $0.38 \mu$  was measured at two windows. At this wavelength,

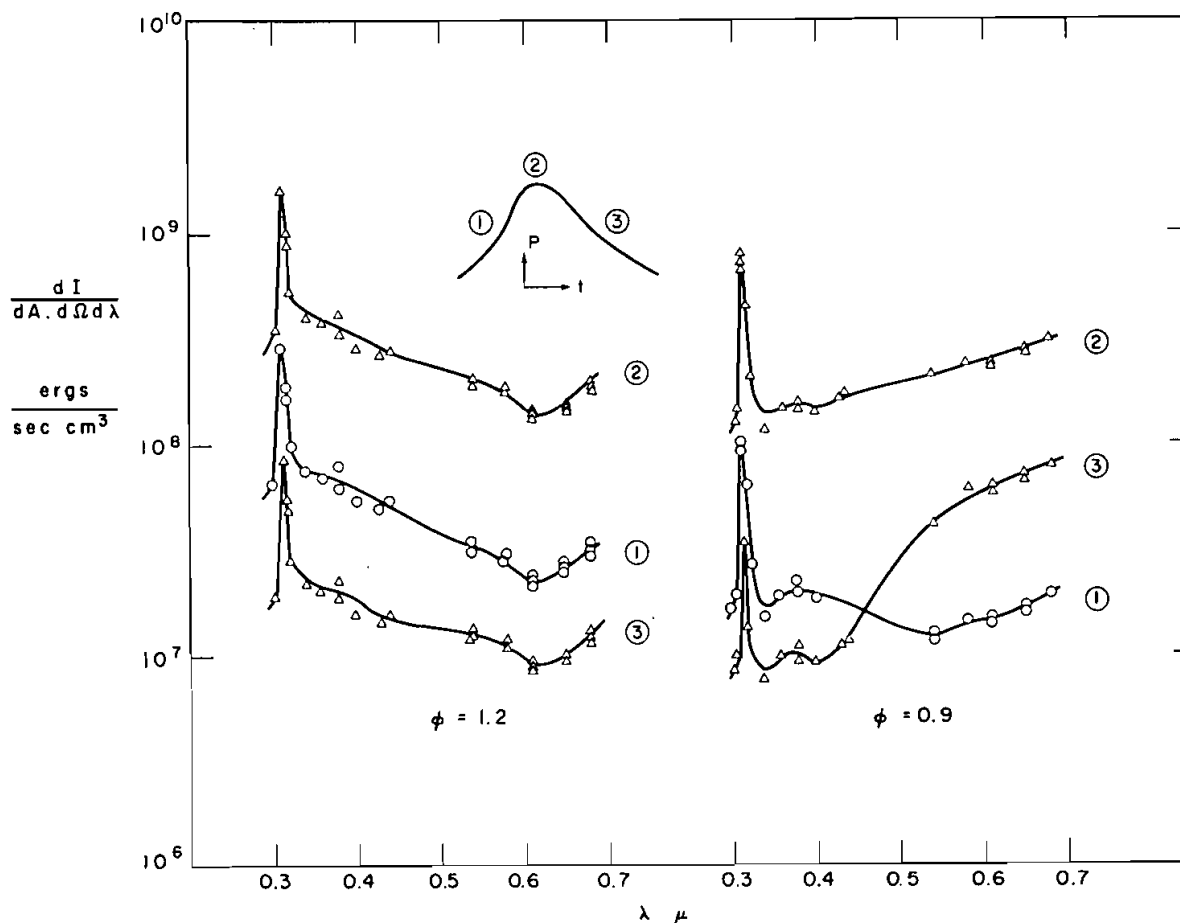


FIG. 11. Spectral intensity observed at three consecutive times during the cycle, before, at, and after peak pressure as shown by the corresponding circled numbers on the pressure-time schematic.

as can be seen from the photographic spectra Figure 8, the radiation is free from discrete contributions and should represent the CO—O continuum. If this is so the radiation can be used to give an instantaneous temperature as outlined in Section V(1). The temperatures determined in this way were compared with those calculated using the unmixed model of Section II and the known pressure curves. The two temperatures agreed absolutely to within the accuracy of the radiation constant and the experimental residual gas fraction. The measured temperatures showed the expected nearly isentropic compression and expansion as well as a temperature difference of  $\sim 50^\circ\text{K}$  between the two windows.

In the second experiment, nitric oxide was added to the airflow in known amounts, and the change in radiation was measured. The extra radiation was

proportional to the added nitric oxide and had the same shape as that observed when no nitric oxide is added. The effect of adding nitric oxide to the airflow is shown in Figure 12 where data records are displayed for two cycles, similar in every respect except for the amount of nitric oxide added. The traces of radiation intensity at  $0.38\ \mu$  are effectively alike, but the traces at  $0.61\ \mu$  and  $0.68\ \mu$  for nitric oxide added show a much larger jump in radiation at the front than for no nitric oxide added.

The radiation intensities occurring just after the reaction zone for a number of data records are plotted against per cent nitric oxide added in Figure 13. For clarity, only the data points for  $0.54\ \mu$  are shown. The straight lines are least squares fits to data with similar scatter. The figure shows that for all practical purposes the radiation at  $0.38\ \mu$ , and hence the temperature after the reaction

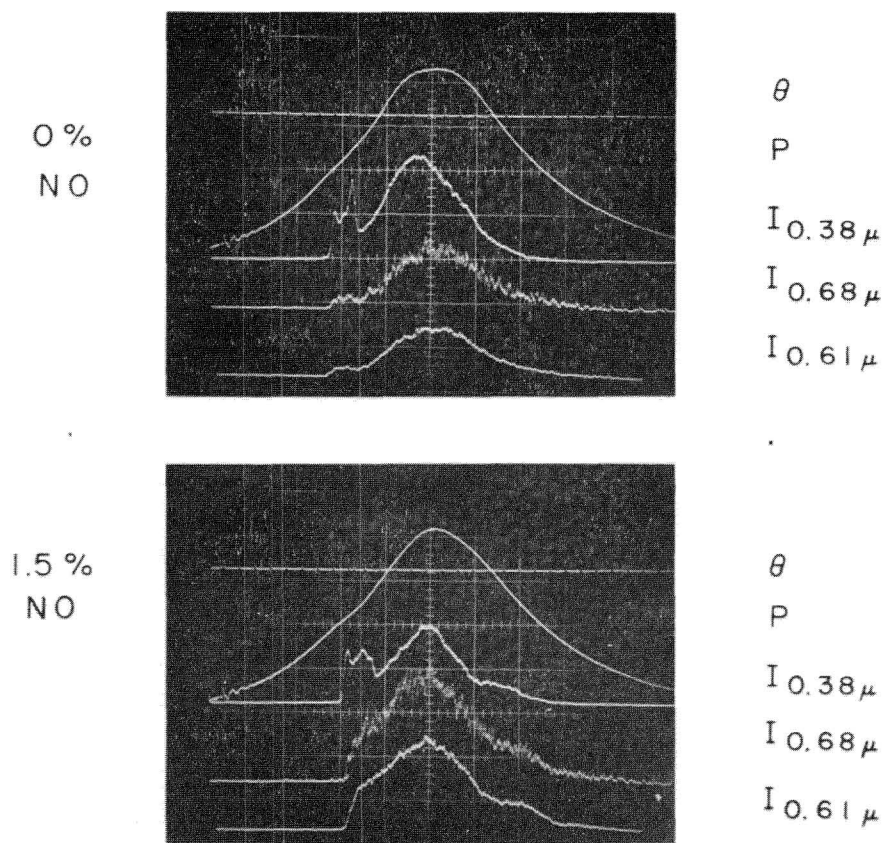


FIG. 12. Two data records showing effect of NO addition. Upper record is for no NO added; lower record is for 1.5% NO added.

zone is unaffected by nitric oxide addition. At the other wavelengths the radiation is proportional to the amount of nitric oxide added. The fact that the intercepts are not zero is probably due to the presence of some nitric oxide just after the reaction zone, either left over from the previous cycle as residual or created in the front. There is also a constant contribution to the radiation from the long wavelength end of the CO—O continuum and from water vapor at  $0.75 \mu$ . In any event the shape of the radiation that is proportional to nitric oxide added is given by the slopes of the lines. These slopes are shown in Figure 14.

In systems where  $\text{NO}_2$  exists as well as NO and O, in addition to the NO—O chemiluminescence radiation,  $I_{\text{NO}} \propto [\text{NO}][\text{O}]$ , there is thermal radiation from  $\text{NO}_2$ . Since the shapes of the two spectra are known, Fontijn *et al.* (1964), Levitt (1965), and are different, the two components can in principle be separated. Figure 14 shows the slope data in relation to these two continuum shapes,  $f$  being the

fraction of radiation at  $0.61 \mu$  due to the chemiluminescent radiation. Although the predicted value of  $f$  is 0.75 based on the published rates and the equilibrium ratio of NO to  $\text{NO}_2$  for this temperature, a value of  $f = 0.4$  fits the data better and is not in serious disagreement considering the uncertainties in the shapes and the radiation constants relative to one another. The value of  $f = 0.4$  was not observed to vary, to within the experimental error, throughout the range of conditions encountered in the experiment (rich and lean, nitric oxide added and not added) and has been taken to be constant for data reduction.

### 3. Data Reduction

In principle, simultaneous recording of pressure and light intensities at a given location from two wavelengths representing the CO—O and NO—O continua, yields the temperature, CO, O, and NO concentrations as outlined in Section V(1). In practice, measurements from a given single cycle

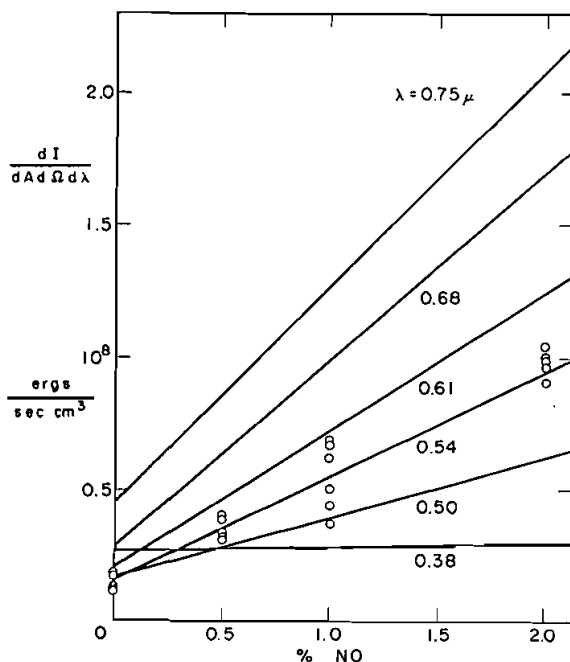


FIG. 13. Radiation intensity observed just after the reaction zone at various wavelengths plotted against percent NO added. For clarity only points for  $0.54 \mu$  are shown.

show a great deal of scatter due to the fact that the optical paths for the four channels are not coincident on a scale of mm's, and on this scale there are significant turbulent fluctuations in temperature. As a result it was necessary to average data from a number of selected cycles.

Because of the cycle to cycle variation in pressure, burning velocity, and the resulting exponential cycle to cycle light intensity variation, a straight forward random selection of cycles was unsuitable. Instead cycles were chosen on the basis of peak pressure, selecting only those cycles with peak pressure within  $\pm 10$  psi of the chosen pressure. The resulting flame arrival times were within 5 crank-angle degrees of one another, and the light intensities at a given wavelength for the rest of the cycle excluding the flame reaction zone were within a  $\pm 30$  per cent band on either side of a smooth line drawn through the data. Average intensity at  $0.38 \mu$  is used to represent the CO—O continuum, and the average intensity at  $0.61 \mu$ , after correction for the underlying CO—O continuum and multiplication by  $f = 0.4$  for the presence of  $\text{NO}_2$ , is used to represent the NO—O continuum. Then as outlined in Section V(1) values of temperature, CO, O,

and NO can be calculated as a function of time during the cycle.

#### 4. Results

The results of such calculations are given in Figures 15 and 16 where experimental nitric oxide concentrations are shown versus time and crank angle for lean conditions  $\phi = 0.9$ . The error bars are  $\pm 30$  per cent corresponding to the scatter in averaging and  $F$  indicates flame arrival time. Displayed also are the rate-limited computer solutions for parts of the charge that burned early and late in the cycle.

Figure 15 shows a comparison between nitric oxide concentrations observed at two different windows,  $W_2$  being closer to the spark than  $W_3$ , and shows higher nitric oxide due to higher temperatures. Both curves exhibit the expected nonequilibrium behavior and fall within the predicted limits. No significant amount of nitric oxide is produced at the flame front under these conditions.

In Figure 16 measured nitric oxide is plotted for both 0 per cent and 1.0 per cent added nitric oxide as seen at  $W_3$ . The temperature and reaction rates

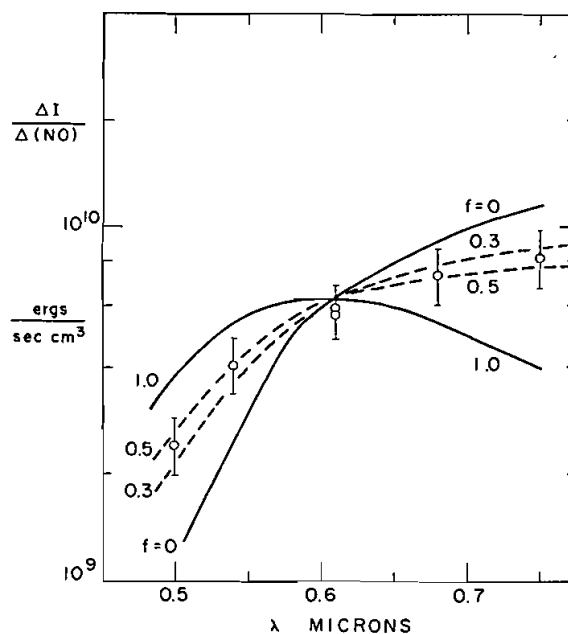


FIG. 14. Incremental intensities per mole fraction of added NO plotted against wavelength compared with theoretical shapes. The solid curves are the shapes of the chemiluminescence radiation  $f = 1.0$ , and thermal radiation  $f = 0$  where  $f$  is the fraction of total radiation at  $0.61 \mu$  due to the chemiluminescent component.

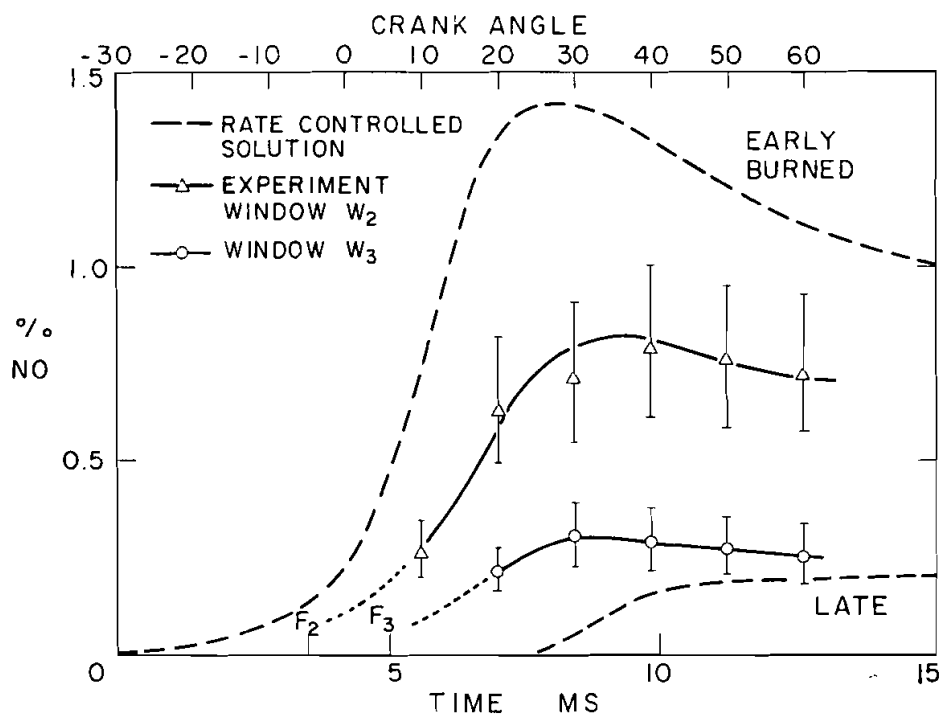


FIG. 15. Experimental NO concentrations observed at two windows.  $W_2$  is closer to the spark than  $W_3$ . Dotted curves are computer solutions for the kinetic NO behavior of early and late burned gas,  $\phi = 0.9$ .

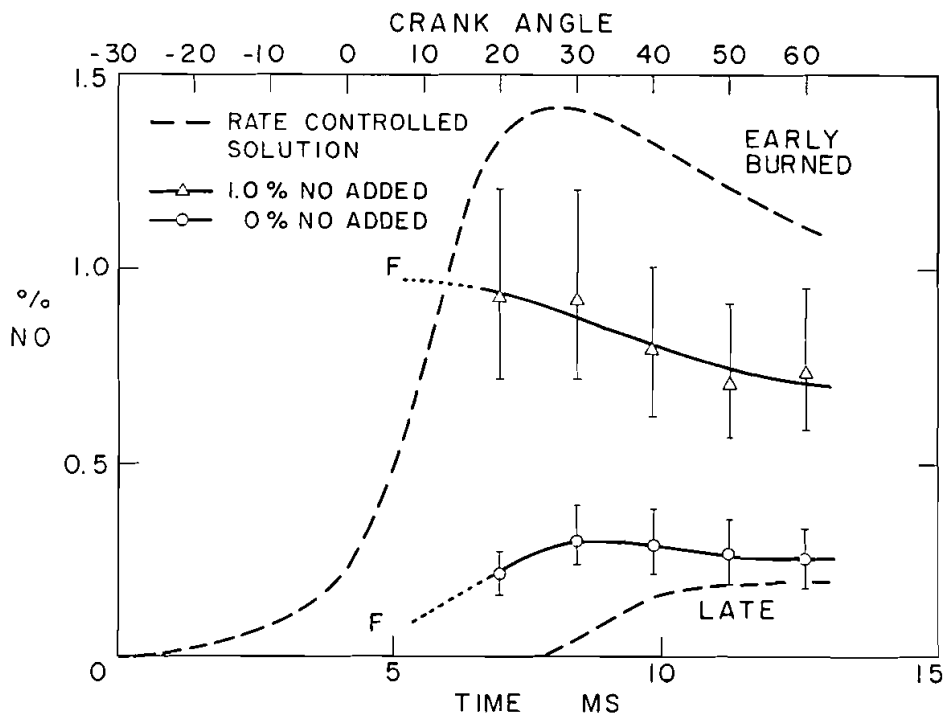


FIG. 16. Experimental NO concentrations at  $W_3$  with and without NO added. Kinetic solutions are shown,  $\phi = 0.9$ .

are low enough so that not much nitric oxide is produced in the 0 per cent added case or decomposed in the 1.0 per cent added case.

At present only the data for lean conditions has been analysed, but there do not appear to be any qualitative differences for rich conditions, and work is progressing on their analysis.

## VI. CONCLUSIONS

The time-resolved experimental measurements and the data reduction described in this paper confirm that these features should be included in models used to predict the nitric oxide concentrations found in spark ignition engines.

1. Both the formation and decomposition of nitric oxide in the post-flame gases are rate limited at the conditions under which I.C. engines normally operate.

2. At least in the lean case, the nitric oxide formed in the flame front is negligible.

3. The state of the burned gas is not uniform; a substantial temperature gradient, and hence nitric oxide concentration gradient exists behind the flame zone.

*This work was supported in part by the M.I.T. Urban Systems Laboratory from the Ford Urban Grant, by the Sloan Basic Research Fund, and by the Ford Foundation Fund.*

## REFERENCES

- Alperstein, M. and Bradow, R. L., 1966, Exhaust Emissions Related to Engine Combustion Reactions, paper presented at Fuels and Lubricants Meeting, SAE paper 660781.
- Campbell, I. M. and Thrush, B. A., 1968, Reactivity of Hydrogen to Atomic Nitrogen and Atomic Oxygen, *Trans. Faraday Soc.* **64**, Part 5, 1265-1274.
- Eyzat, P. and Guibet, J. C., 1968, A New Look at Nitrogen Oxides Formation in Internal Combustion Engines, SAE paper 680124, presented at Automotive Engineering Congress.
- Fontijn, A., Meyer, C. F. and Schiff, H. I., 1964, Absolute Quantum Yield Measurements of the NO—O Reaction and Its Use as a Standard for Chemiluminescent Reactions, *J. Chem. Phys.* **40**, 64.
- Hartunian, R. A., Thompson, W. P. and Hewitt, E. W., 1966, Glow-Discharge Shock Tube for Studying Chemiluminescent, Surface-Catalytic, and Gas-Phase Reaction Rates; Temperature Dependence of NO—O and CO—O Chemiluminescence, *J. Chem. Phys.* **44**, 1765.
- Hazen, D. F. and Holiday, G. W., 1962, The Effects of Engine Operating and Design Variables on Exhaust Emissions, SAE paper 486C presented at SAE National Automobile Week.
- Huls, T. A. and Nickol, H. A., 1967, Influence of Engine Variables on Exhaust Oxides of Nitrogen Concentrations from a Multi-cylinder Engine, SAE paper 670482 presented Mid-year Meeting.
- Levitt, B. P., 1965, Temperature and Wavelength Dependence of the Thermal Emission and O—NO Recombination Spectra of NO<sub>2</sub>, *J. Chem. Phys.* **42**, 1038.
- Newhall, H. K., 1968, Kinetics of Engine-Generated Nitrogen Oxides and Carbon Monoxide, 12th Symposium (International) on Combustion, The Combustion Institute.
- Newhall, H. K. and Starkman, E. S., 1967, Direct Spectroscopic Determination of Nitric Oxide in Reciprocating Engine Cycles, Paper 670122 presented at SAE Automotive Engineering Congress.
- Myers, B. F. and Bartle, E. R., 1967, Shock-Tube Study of the Radiative Processes in Systems Containing Atomic Oxygen and Carbon Monoxide at High Temperature, *J. Chem. Phys.* **47**, 1783.
- Rassweiler, G. M. and Withrow, L., 1935, Flame Temperatures Vary with Knock and Combustion Chamber Position, *SAE Trans.*, 125-133.
- Schofield, K., 1967, An Evaluation of Kinetic Rate Data for Reactions of Neutrals of Atmospheric Interest, *Planet. Space Sci.* **15**, 643-670.
- Wimmer, D. B. and McReynolds, L. A., 1961, Nitrogen Oxides and Engine Combustion, Paper 380E presented at SAE Summer Meeting.
- Zeldovich, Y. B., 1946, The Oxidation of Nitrogen in Combustion Explosions, *Acta Physicochimica U.S.S.R.* **21**, 577-628.